

Review

# Research Progress of Co-Catalysts in Photocatalytic CO<sub>2</sub> Reduction: A Review of Developments, Opportunities, and Directions

Cheng Zuo , Qian Su \*  and Xueyuan Yan \* 

College of Chemical Engineering and Environmental Engineering, Weifang University, Weifang 261061, China

\* Correspondence: suqian93@163.com (Q.S.); yanxueyuan@wfu.edu.cn (X.Y.)

**Abstract:** With the development of the global economy, large amounts of fossil fuels are being burned, causing a severe energy crisis and climate change. Photocatalytic CO<sub>2</sub> reduction is a clean and environmentally friendly method to convert CO<sub>2</sub> into hydrocarbon fuel, providing a feasible solution to the global energy crisis and climate problems. Photocatalytic CO<sub>2</sub> reduction has three key steps: solar energy absorption, electron transfer, and CO<sub>2</sub> catalytic reduction. The previous literature has obtained many significant results around the first two steps, while in the third step, there are few results due to the need to add a co-catalyst. In general, the co-catalysts have three essential roles: (1) promoting the separation of photoexcited electron–hole pairs, (2) inhibiting side reactions, and (3) improving the selectivity of target products. This paper summarizes different types of photocatalysts for photocatalytic CO<sub>2</sub> reduction, the reaction mechanisms are illustrated, and the application prospects are prospected.

**Keywords:** CO<sub>2</sub> reduction; co-catalysts; fossil fuels; electron–hole pairs; precious metal



**Citation:** Zuo, C.; Su, Q.; Yan, X. Research Progress of Co-Catalysts in Photocatalytic CO<sub>2</sub> Reduction: A Review of Developments, Opportunities, and Directions. *Processes* **2023**, *11*, 867. <https://doi.org/10.3390/pr11030867>

Academic Editors: Wende Tian, Qingjie Guo, Bin Liu and Zhe Cui

Received: 13 February 2023

Revised: 8 March 2023

Accepted: 12 March 2023

Published: 14 March 2023



**Copyright:** © 2023 by the authors. Licensee MDPI, Basel, Switzerland. This article is an open access article distributed under the terms and conditions of the Creative Commons Attribution (CC BY) license (<https://creativecommons.org/licenses/by/4.0/>).

## 1. Introduction

With the rapid economic development of the world, large amounts of fossil fuels are consumed. As a result, a large amount of CO<sub>2</sub> is discharged into the air, causing the greenhouse effect, thus breaking the ecological balance in the world. Fossil fuels are non-renewable energy [1,2]. In contrast, solar energy is inexhaustible, providing the earth with about 120,000 TW of energy annually [3,4]. How to improve the conversion and utilization of solar energy has always been the focus of researchers. In the photocatalytic process (Figure 1), semiconductor (SC) photocatalysts could be stimulated by the absorbed photons to produce e<sup>−</sup>–h<sup>+</sup> pairs, and after absorbing the photon energy, the internal electrons will be transferred from the valence band (VB) to the conduction band (CB) inside the semiconductor [5–7]. Negatively charged electrons are produced at the CB, and positively charged holes are produced at the VB. Subsequently, the light-induced e<sup>−</sup> and h<sup>+</sup> will separate and migrate to the photocatalyst surface. The reactants adsorbed on the inner surface of the semiconductor undergo a redox reaction for energy conversion [8–10].

Fujishima et al. [11]’s preliminary research on photocatalysts shows that TiO<sub>2</sub> electrodes could make CO<sub>2</sub> conversion to small amounts of methanol under sunlight, which makes scholars focus on photocatalysis technology. Common semiconductors like metal oxides (e.g., TiO<sub>2</sub> and Ga<sub>2</sub>O<sub>3</sub>) and metal sulfides (e.g., CdS and MoS<sub>2</sub>) have been found [1,3,6]. In general, photocatalytic CO<sub>2</sub> conversion can be roughly divided into three processes [9,10]. At present, much research has been completed on the two processes (i and ii), and process (iii) could improve catalytic efficiency by adding co-catalysts. Meanwhile, it improves the selectivity of CO<sub>2</sub> reduction products and inhibits side reactions. Up until now, research on co-catalyst photocatalytic CO<sub>2</sub> has been rare.

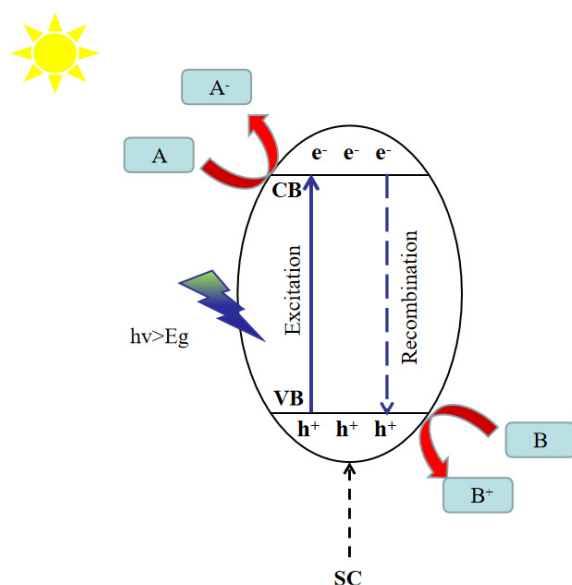


**Figure 1.** The mechanism of the photocatalytic process.

Up to now, CO<sub>2</sub> reduction catalysts could be divided into two categories: precious metal-based catalysts and precious metal-free catalysts. The precious metal-based catalysts showed excellent stability and redox properties in photocatalytic CO<sub>2</sub> reduction, such as Pt [12–20], Ag [21–31], Pd [32–36], Ru [37–39], Rh [40,41], Au [42,43], and alloys [44–47]. These catalysts have been widely applied to improve the selectivity of photocatalytic CO<sub>2</sub> reduction products. In addition, the exposed crystal surface, particle size, and particle distribution greatly affect the activity and selectivity of photocatalytic CO<sub>2</sub> reduction [48].

While the high cost of precious metal catalysts has limited their development for industrial applications, the search for low-cost, high-activity catalysts has become the focus of current research. The precious metal-free catalysts include Cu/Cu<sub>2</sub>O/CuO [49–60], Fe/Fe<sub>2</sub>O<sub>3</sub> [61], Ni/NiO [62–67], co-incorporated metal-organic framework (MOF), and carbon nanomaterials. Cu/Cu<sub>2</sub>O/CuO was recognized as an excellent catalyst with high activity. Zhang et al. [68] added unsaturated monatomic Co to the MOF system to improve photocatalytic CO<sub>2</sub> reduction efficiency.

Although researchers have made many contributions to the photocatalytic reduction of CO<sub>2</sub>, comprehensive reviews are still necessary to provide direction for future research. In this paper, we will focus on the mechanism and role of co-catalysts in CO<sub>2</sub> photocatalytic reduction reactions.

## 2. Application of Co-Catalysts in CO<sub>2</sub> Photocatalytic Reduction

### 2.1. Catalytic Reduction of CO<sub>2</sub> Reaction Mechanism

Due to the linear structure of CO<sub>2</sub>, the energy required to cleave the C–O bond was much higher than that required to cleave the C–C, C–O, and C–H bonds [69]. In addition, the relatively wide energy gap and electron affinity of CO<sub>2</sub> leads to a negative single-electron transfer redox potential. Therefore, different reaction pathways have been developed to reduce CO<sub>2</sub> at lower energies. In general, the photocatalytic CO<sub>2</sub> reduction process must follow the following four steps [70,71]: (1) the electrons on the photocatalyst VB are stimulated and transferred to its CB to generate a photogenerated charge, and the photogenerated charge could either be transferred separately to the photocatalyst surface for photocatalytic reaction or recombined to release photons or heat; (2) the catalyst surface for CO<sub>2</sub> absorption; (3) photogenerated electrons on the photocatalyst surface to convert CO<sub>2</sub> into fuel; and (4) desorption of photocatalyst products. A conductive potential that is more negative than the required standard potential and effective electron transfer to the CO<sub>2</sub>-adsorbed semiconductor surface determine the efficiency of CO<sub>2</sub> reduction (Table 1).

**Table 1.** Different reduction products obtained from the photocatalytic reduction of CO<sub>2</sub> in an aqueous solution and the corresponding electrode potentials (vs. standard hydrogen electrode, 25 °C, pH = 7).

Reaction	E <sup>0</sup> <sub>redox</sub> (vs. NHE)/V
CO <sub>2</sub> + 2H <sup>+</sup> + 2e <sup>-</sup> → HCOOH	-0.61
CO <sub>2</sub> + 2H <sup>+</sup> + 2e <sup>-</sup> → CO + H <sub>2</sub> O	-0.53
CO <sub>2</sub> + 4H <sup>+</sup> + 4e <sup>-</sup> → HCHO + H <sub>2</sub> O	-0.48
CO <sub>2</sub> + 4H <sup>+</sup> + 4e <sup>-</sup> → C + 2H <sub>2</sub> O	-0.20
CO <sub>2</sub> + 6H <sup>+</sup> + 6e <sup>-</sup> → CH <sub>3</sub> OH + H <sub>2</sub> O	-0.38
CO <sub>2</sub> + 8H <sup>+</sup> + 8e <sup>-</sup> → CH <sub>4</sub> + 2H <sub>2</sub> O	-0.24
2CO <sub>2</sub> + 12H <sup>+</sup> + 12e <sup>-</sup> → C <sub>2</sub> H <sub>4</sub> + 4H <sub>2</sub> O	-0.34
2CO <sub>2</sub> + 12H <sup>+</sup> + 12e <sup>-</sup> → C <sub>2</sub> H <sub>5</sub> OH + 3H <sub>2</sub> O	-0.33
2CO <sub>2</sub> + 14H <sup>+</sup> + 14e <sup>-</sup> → HCOOH + C <sub>2</sub> H <sub>6</sub>	-0.27
2H <sup>+</sup> + 2e <sup>-</sup> → H <sub>2</sub>	-0.42

The products obtained change with the change of reaction conditions and catalytic materials during the reduction process. The photon energy required for photoexcitation depends on the band gap of the photocatalyst. The edge position of the photocatalyst's energy band should match the relevant reaction's redox potential. The different reduction products and corresponding electrode potentials obtained from the photocatalytic reduction reaction of CO<sub>2</sub> in an aqueous solution are shown in Table 1. The ideal CO<sub>2</sub> photocatalytic reduction reaction must meet the requirement that the CB potential of photogenerated electrons is more negative than the potential of the reduction products/CO<sub>2</sub> (CH<sub>4</sub>/CO<sub>2</sub>, CH<sub>3</sub>OH/CO<sub>2</sub>, HCHO/CO<sub>2</sub>, HCOOH/CO<sub>2</sub>, or CO/CO<sub>2</sub>), and the VB that generates holes is corrected than the potential of the oxidation reaction (O<sub>2</sub>/H<sub>2</sub>O) of H<sub>2</sub>O. To sum up, photocatalytic reduction of CO<sub>2</sub> must meet two conditions: (i) photon energy is greater than or equal to band gap energy and (ii) the CB potential is more negative than the surface electron acceptor potential, and the VB potential is corrected than the surface electron donor potential. In this way, the reaction process of photocatalytic reduction of CO<sub>2</sub> can be realized [72].

#### Mechanistic Role of Co-Catalysts in CO<sub>2</sub> Photocatalytic Reduction

In the process of photocatalytic CO<sub>2</sub> reduction, the co-catalyst plays three critical roles in participating in the reaction as follows: (i) co-catalysts could reduce the activation energy or the reaction barrier on the semiconductor surface, (ii) co-catalysts could rapidly separate and migrate holes and electron pairs on semiconductor surfaces, and (iii) the co-catalyst could inhibit the side reactions in the photocatalytic reduction of CO<sub>2</sub> and improve the selectivity of the target product.

Photoexcited electrons could migrate through the photocatalyst conduction band to the co-catalyst surface to reduce CO<sub>2</sub> to CO, HCOOH, HCHO, CH<sub>3</sub>OH, and CH<sub>4</sub> (from Figure 2). The excellent heterojunction structure between the co-catalyst and the semiconductor is vital for enhancing the migration of photogenerated carriers from the semiconductor to the co-catalyst.

In the process of photocatalytic CO<sub>2</sub> reduction, many factors affect the activity of the co-catalyst. For instance, elemental composition, crystal structure, exposed crystalline surface, and particle size. Excessive co-catalysts could have the following three problems: (i) Excess co-catalyst could cover the active sites on the semiconductor surface and hinder the reduction of CO<sub>2</sub>. (ii) Excess co-catalysts block sunlight and reduce light absorption, thus reducing the number of hole–electron pairs. (iii) Excessive amount of co-catalyst could cover the semiconductor surface unevenly, resulting in a larger catalyst size and thus lower catalytic activity. Therefore, finding the optimal amount of co-catalyst addition is necessary to maximize the photocatalyst activity.

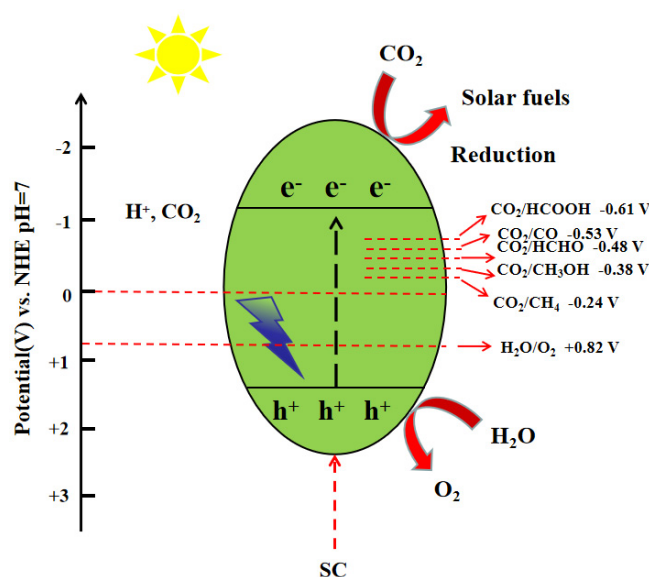


Figure 2. Mechanism of photocatalytic CO<sub>2</sub> reduction.

### 3. Noble Metal-Based Co-Catalysts

Precious metal-based co-catalysts, such as Pt, Ag, Pd, Rh, Au, and alloys, have successfully improved the activity and selectivity of target products for photocatalytic CO<sub>2</sub> reduction in a range of photocatalyst systems. Noble metal co-catalysts improve the photocatalytic efficiency and enhance the selectivity of target products in the photocatalytic reduction of CO<sub>2</sub>. However, the high cost of the precious metal itself limits its industrial development process.

#### 3.1. Pt-Based Co-Catalysts

Generally, there are two main categories of Pt distribution on the photocatalyst surface. One is the in situ loading of Pt during the synthesis of TiO<sub>2</sub> photocatalysts, and the other is the effect of Pt on the synthesis of TiO<sub>2</sub> photocatalysts. The researchers [12] synthesized TiO<sub>2</sub> nanofibers (NFs) using Au and Pt NP coatings by a simple electron spin method. The precursors containing Ti, Au, and Pt were mixed, respectively. The Au and Pt NPs were found to bind precisely to TiO<sub>2</sub> in situ during the electron spin. The Au- and Pt-loaded TiO<sub>2</sub> NFs exhibited higher CO<sub>2</sub> reduction activity under the action of H<sub>2</sub>O vapor than pure TiO<sub>2</sub>.

In the preparation of TiO<sub>2</sub>, in addition to the above two methods, impregnation–calcination and microwave-assisted solvent-heat treatment methods were used. The mesoporous TiO<sub>2</sub> loaded with Pt, Au, and Ag exhibited photocatalytic activity for reducing CO<sub>2</sub> to gas-phase CH<sub>4</sub> under visible light irradiation. The mesoporous TiO<sub>2</sub> loaded with 0.2% Pt by mass fraction produced the highest CH<sub>4</sub> content of 5.7 μmol g<sup>-1</sup> after visible light irradiation for 2 h. The reason is that the noble metal Pt has the highest work function (5.65 eV) and the lowest Fermi energy level among many co-catalysts. It has the most potent electron extraction ability, making it an ideal choice for photocatalytic CO<sub>2</sub> reduction co-catalyst. Therefore, adding co-catalyst Pt on the semiconductor surface could increase electron mobility and maximize the separation of electrons and holes [73]. Among them, the loading of Pt into TiO<sub>2</sub> was the most widely studied. Pt, Au, and Ag were loaded onto the mesoporous TiO<sub>2</sub> surface. The results showed that when the mass fraction of Pt was 0.2%, the highest yield of CH<sub>4</sub> was 5.7 μmol g<sup>-1</sup> after 2 h of light exposure. The possible reason is that the value of the work function of Pt is higher than that of Au (5.1 eV) and Ag (4.26 eV). Therefore, photogenerated electrons could migrate from TiO<sub>2</sub> to Pt. Furthermore, Xie et al. [15] reported various noble metals loaded on TiO<sub>2</sub>. The results showed that the noble metals are active in the order of Ag < Rh < Au < Pd < Pt through the yield of CH<sub>4</sub>. This trend is consistent with the respective functionalities of the metals. Although the

addition of noble metal catalysts improved the selectivity of  $\text{CH}_4$ , the selectivity of CO (e.g., noble metal Rh) decreased instead. It also accelerates the trend of  $\text{H}_2\text{O}$  reduction to  $\text{H}_2$ . The results show that the selectivity of  $\text{CO}_2$  reduction decreases from 56% for  $\text{TiO}_2$  to 39–45% for the loaded noble metal in  $\text{TiO}_2$ . Therefore, the focus of current research is the study of how to improve activity.

The impregnation roasting technique was also widely used for Pt-loaded  $\text{TiO}_2$ . For example, using impregnation and calcination methods, Anpo et al. [17] loaded a mass fraction of 1.0% Pt onto synthesized  $\text{TiO}_2$ -anchored Y zeolites. The addition of Pt increased the  $\text{CH}_4$  yield and decreased in  $\text{CH}_3\text{OH}$  yield. Furthermore, a microwave-assisted solvothermal rapid loading of Pt on  $\text{TiO}_2$  was developed [18]. For example, the highest photocatalytic activity for CO and  $\text{CH}_4$  was achieved when the mass fraction of Pt was 0.6%. At the same time, undoped  $\text{TiO}_2$  was 0.20% and 0.34%. The excess Pt loading reduced the dispersion of Pt NPs and increased the size of Pt NPs. It was easier to remove from the  $\text{TiO}_2$  NTAs higher than other polyols. Under visible light irradiation, the Pt-loaded  $\text{TiO}_2$  NTAs exhibit a  $\text{CH}_4$  content of about  $25 \pm 4$  ppm in  $\text{CO}_2$  and  $\text{H}_2\text{O}$  vapor, while the unloaded  $\text{TiO}_2$  NTAs produce only about 3 ppm of  $\text{CH}_4$ . The Pt NPs were uniformly dispersed on the surface of  $\text{TiO}_2$  NTAs, providing many active sites and enhancing the photocatalytic activity of  $\text{TiO}_2$  NTAs.

Due to quantum confinement, the deposition time may lead to tiny Pt NPs high energy band separation, thus limiting the electron transfer from  $\text{TiO}_2$  to Pt (Figure 3) [74]. On the contrary, the larger the Pt NPs have similar energy band positions as the bulk Pt. In this case, the light-induced migration of electrons and holes to Pt leads to their recombination. The Pt NPs with optimal size and energy band between  $-4.4$  and  $-5.65$  eV can promote efficient photoinduced electron transfer from  $\text{TiO}_2$  only when the appropriate deposition time is used (Figure 3).

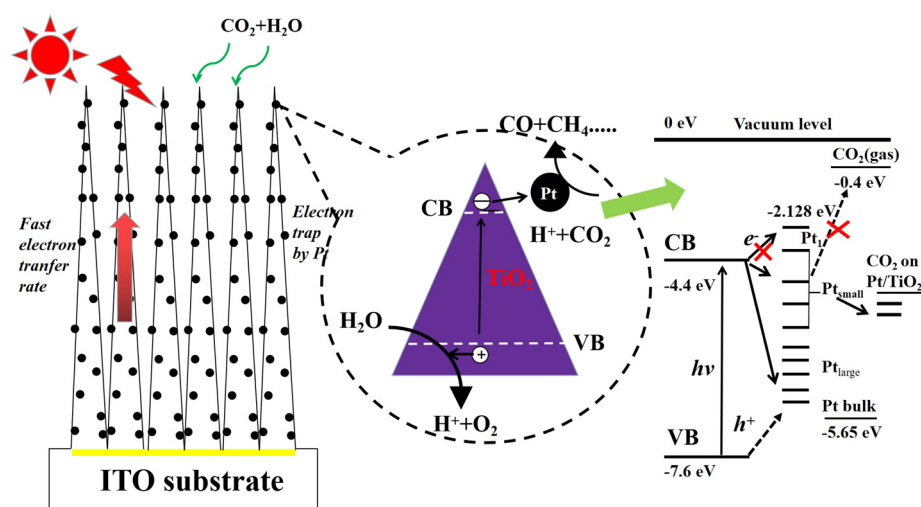


Figure 3. Mechanism diagram of  $\text{CO}_2$  reduction by Pt- $\text{TiO}_2$  photocatalyst [74].

Yuan et al. [75] loaded 0.5% Pt by mass fraction onto P/ $g\text{-C}_3\text{N}_4$  composites and exhibited excellent activity. Cao et al. [76] loaded Pt co-catalysts onto  $\text{In}_2\text{O}_3$  nanocrystal-deposited  $g\text{-C}_3\text{N}_4$  NSs hybrid photocatalysts. After 4 h of visible light irradiation, the yield of  $\text{CH}_4$  reached 159.2 ppm. Whereas the catalyst not loaded with  $\text{In}_2\text{O}_3/g\text{-C}_3\text{N}_4$  was only 76.7 ppm. Pt could act as an electron receiver and facilitate charge transfer and migration. Li et al. [77] used  $\text{H}_2\text{O}$  vapor to photocatalysis the reduction of  $\text{CO}_2$  to  $\text{CH}_4$  by photodeposition with Pt loaded on  $\text{SiO}_2$  columnar  $\text{HNb}_3\text{O}_8$ . The highest photocatalytic activity for  $\text{CH}_4$  was achieved when the mass fraction of Pt was 0.4%. The results showed that at 0.4 wt% Pt/ $\text{SiO}_2\text{-HNb}_3\text{O}_8$  in the presence of  $\text{H}_2\text{O}$  vapor and  $\text{N}_2$ , there was no  $\text{CO}_2$  in the product, indicating that part of the  $\text{CH}_4$  may come from carbon accumulation on

the photocatalyst. In comparison, the rate of  $\text{CH}_4$  generation from carbon accumulation is much lower than the rate of  $\text{CH}_4$  generation.

Although Pt is a more applied co-catalyst in the photocatalytic reduction of  $\text{CO}_2$  for hydrogen production, it was not the best. This was because it permanently traps photogenerated electrons while promoting  $\text{H}_2$  production, which will reduce the efficiency of photocatalytic  $\text{CO}_2$  reduction [18,72]. In addition, Pt could increase the activity of  $\text{CO}_2$  conversion to  $\text{CH}_4$  more than  $\text{CO}$  because the generated  $\text{CO}$  cannot be desorbed from Pt. It leads to catalyst deactivation [78].

In addition, it was also found that when an excessive amount of Pt was loaded onto  $\text{TiO}_2$ , Pt would be loudly agglomerated on the semiconductor surface. The electron-rich density of Pt will hinder the formation of Schottky barriers between  $\text{TiO}_2$  and Pt, which may increase the electron–hole complex probability and ultimately reduce the  $\text{CO}_2$  conversion efficiency [78].

### 3.2. Ag-Based Co-Catalysts

The binding energy of Ag to  $\text{CO}$  is much lower than that of Pt to  $\text{CO}$ , and  $\text{CO}$  is more easily desorbed from the Ag surface for  $\text{CO}_2$  reduction conversion. Therefore, Ag was widely used as a co-catalyst for  $\text{CO}_2$  photocatalytic reduction, especially in improving the selectivity of  $\text{CO}$ . The researchers loaded the co-catalyst Ag onto  $\text{TiO}_2$ . Reduction products were mainly  $\text{CH}_4$  and  $\text{CH}_3\text{OH}$ . Experimental results showed that when the mass fraction of Ag exceeded 5%, Ag clusters would be formed on the semiconductor surface, strengthening the formation of Schottky barriers. It causes the separation of electron–hole pairs and prolongs the lifetime of electron–hole pairs, thus improving the catalyst activity [79].

Researchers [80] added a series of co-catalysts to the synthesized  $\text{BaLa}_4\text{Ti}_4\text{O}_{15}$ , respectively. After experiments, it was found that NiO, Ru, and Au could improve the activity of photocatalytic synthesis of  $\text{H}_2$  and did not achieve  $\text{CO}_2$  reduction because these three precious metals mainly act in the photocatalytic decomposition of  $\text{H}_2\text{O}$  to  $\text{H}_2$ . In contrast, Ag is the most effective co-catalyst for promoting  $\text{CO}_2$  reduction on  $\text{BaLa}_4\text{Ti}_4\text{O}_{15}$  (Figure 4).

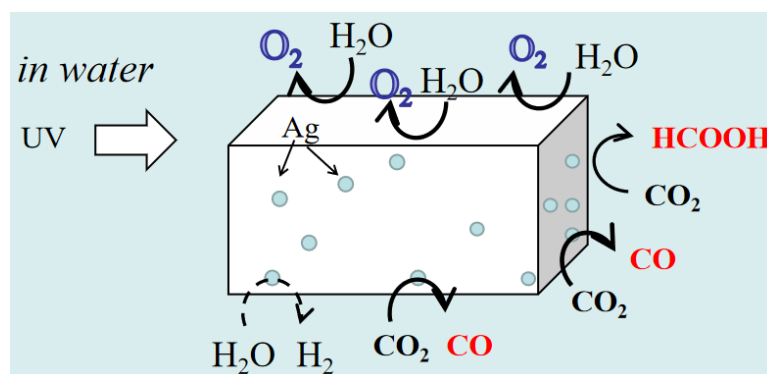


**Figure 4.** Mechanism of photocatalytic reduction of  $\text{CO}_2$  by Ag-loaded  $\text{BaLa}_4\text{Ti}_4\text{O}_{15}$  [80].

There are four methods for loading Ag onto  $\text{BaLa}_4\text{Ti}_4\text{O}_{15}$ : impregnation, photolytic deposition,  $\text{H}_2$  reduction, and liquid-phase reduction. Among them, the liquid-phase reduction method is the most efficient yield for the reduction of  $\text{CO}_2$  to  $\text{CO}$  compared to  $\text{H}_2$  production. It is due to the small size and high dispersion of the deposited co-catalyst Ag, as shown in Figure 4.  $\text{CO}_2$  could fully react with Ag and improve the activity of the co-catalyst.

The co-catalyst Ag differs from Pt because Pt tends to agglomerate on the semiconductor surface. On the one hand, it covers the active sites on the semiconductor surface, and on the other hand, it reduces the light intensity and the  $\text{CO}_2$  reduction activity. Metal Ag could form small clusters on a nanometer scale, and the smaller the size of the clusters, the stronger the interaction with the carrier and the easier to receive electrons on the d orbitals.

### 3.3. Pd-Based Co-Catalysts

Unlike the first two noble metal co-catalysts, the crystalline surface of Pd has a more significant effect on CO<sub>2</sub> reduction. The researchers loaded Pd on TiO<sub>2</sub> by the photodeposition method and then covered a Nafion layer on Pd-TiO<sub>2</sub>. The Pd-TiO<sub>2</sub> photocatalyst with the Nafion layer overlay has vigorous photocatalytic activity and can reduce CO<sub>2</sub> to CH<sub>4</sub> [33].

Researchers [81] investigated the crystallographic selectivity of Pd co-catalysts using 2D g-C<sub>3</sub>N<sub>4</sub> with low layer thickness. Single-crystal Pd NCs and Pd NTs surrounded by {100} and {111} crystal planes were loaded onto g-C<sub>3</sub>N<sub>4</sub> using the solution-phase in situ growth method. The density functional theory (DFT) simulation results show that g-C<sub>3</sub>N<sub>4</sub> has the function of enhanced charge separation efficiency. While the experimental results also revealed that the selectivity of g-C<sub>3</sub>N<sub>4</sub> loaded with Pd NTs (80%) was significantly higher than that of g-C<sub>3</sub>N<sub>4</sub> loaded with Pd NCs (20%).

### 3.4. Ru-Based Co-Catalysts

It was demonstrated that the metal Ru co-catalyst could reduce CO<sub>2</sub>. Baran et al. [38] loaded metal Ru with a mass fraction of 1.0 onto the nanocrystalline ZnS surface by impregnation. The promoting effect of Ru-loaded co-catalysts may come from the following two aspects: (1) the adsorption of photoexcited electrons by Ru improves the charge separation efficiency and (2) Ru-loaded ZnS enhances the adsorption of CO<sub>2</sub>.

### 3.5. Alloy Co-Catalysts

The alloy co-catalysts Au/Cu [44] and Cu/Pt alloys [45] showed synergistic effects in promoting photocatalytic CO<sub>2</sub> reduction. For example, Au/Cu alloy NPs were loaded onto TiO<sub>2</sub>. In particular, the Au/Cu alloy with a mass fraction of 1.5% (1:2 atomic ratio of Au to Cu) loaded onto TiO<sub>2</sub> has high photocatalytic activity. The selectivity of CH<sub>4</sub> was as high as 97%. It was shown that introducing Cu in Au/Cu-TiO<sub>2</sub> could facilitate the transfer of CB electrons from TiO<sub>2</sub> to CO<sub>2</sub>.

The photo deposition of Cu/Pt bimetallic shells on periodically modulated double-walled titanium dioxide nanotubes to reduce of CO<sub>2</sub> to low-carbon hydrocarbons. Under simulated solar irradiation conditions, the optimized PMTiNT had an overall maximum hydrocarbon production rate [45].

## 4. Precious Metal-Free Co-Catalysts

Precious metal-free co-catalysts, especially Cu- [49–60] and Ni-based co-catalysts [62–67], have been widely used for photocatalytic CO<sub>2</sub> reduction reactions. The non-precious metal co-catalysts do not exhibit as high photocatalytic efficiency as those of precious metals in the photocatalytic reduction of CO<sub>2</sub>. However, they could reduce the probability of electron–hole complexation. Excellent photocatalytic activity was exhibited. Most importantly, the low cost of the non-precious metal makes industrialization possible.

### 4.1. Cu-Based Co-Catalysts

Currently, Cu-based co-catalysts are widely used for loading various catalysts. For example, TiO<sub>2</sub>, ZnO, ZrO<sub>2</sub>, and CdS et al. were used to enhance catalyst activity. It is shown that Cu was loaded onto TiO<sub>2</sub> by the thermal hydrolysis method. The TiO<sub>2</sub> surface was in the form of clusters of Cu<sub>2</sub>O. Clusters of Cu<sub>2</sub>O have the effect of having electron traps, which inhibit the carrier complex. Tseng et al. [82] employed a sol-gel method to load Cu onto TiO<sub>2</sub>, and the analytical results showed that the presence of Cu was mainly in the form of Cu<sub>2</sub>O. The 2.0 wt% Cu-modified TiO<sub>2</sub> showed more excellent efficiency for the reduction of CO<sub>2</sub> than unloaded TiO<sub>2</sub>. The loaded Cu on TiO<sub>2</sub> could trap photogenerated electrons, thus improving the electron–hole separation efficiency. The researchers reported that CuO<sub>x</sub>-modified TiO<sub>2</sub> exhibited more excellent activity than AgO<sub>x</sub>-modified TiO<sub>2</sub> in reducing CO<sub>2</sub> to CH<sub>3</sub>OH. In both cases, both CuO<sub>x</sub> and AgO<sub>x</sub> trapped photogenerated

electrons and served as active catalytic sites, and thus the activity was higher than that of pure TiO<sub>2</sub> [83].

Tseng and Wu [84] showed experimentally that the chemical state and distribution of Cu species on TiO<sub>2</sub> greatly influence the photocatalytic CO<sub>2</sub> reduction activity. The results showed that the isolated Cu(I) species obtained was the main active site. TiO<sub>2</sub> modified by Cu has a higher activity than TiO<sub>2</sub> modified by Ag. Xie et al. [85] synthesized Cu-loaded TiO<sub>2</sub> by sol-gel method to photocatalysis reduce CO<sub>2</sub> to CH<sub>3</sub>OH. XAS and XPS spectra showed that the higher the dispersion of Cu<sub>2</sub>O on the TiO<sub>2</sub> surface, the better the photocatalytic performance. Cu/TiO<sub>2</sub> catalysts treated with H<sub>2</sub> reduction after the reaction were found to have altered dispersion and oxidation state of Cu on TiO<sub>2</sub> with reduced activity. It is because Cu<sup>+</sup> electron capture was stronger than Cu<sup>2+</sup> due to the higher reduction potential of Cu<sup>2+</sup>. In addition, stability tests were done, and the used CuO/TiO<sub>2</sub> could be regenerated after exposure to air due to the desorption of its surface gas products. The catalyst has excellent stability.

In addition to the methods above for loading Cu-based co-catalysts during the preparation of TiO<sub>2</sub>, the impregnation–calcination method [51,58], the impregnation–calcination method followed by pretreatment [86,87], stirred sonication [88], and microwave-assisted reduction were used to disperse Cu-based co-catalysts on the treated TiO<sub>2</sub>. Adachi et al. loaded a 5% mass fraction of Cu onto the TiO<sub>2</sub> surface by impregnating and calcining in an H<sub>2</sub> atmosphere [89]. The synthesized Cu/TiO<sub>2</sub> was active in the photocatalytic reduction of CO<sub>2</sub> to CH<sub>4</sub>, C<sub>2</sub>H<sub>4</sub>, and C<sub>2</sub>H<sub>6</sub>. The catalyst did not produce methanol or formaldehyde.

#### 4.2. Ni-Based Co-Catalysts

Ni and NiO have also been used for photocatalytic CO<sub>2</sub> reduction. Wang et al. [90] used a sol-gel method to load NiO with InTaO<sub>4</sub> composites. The NiO co-catalyst was used in conjunction with InTaO<sub>4</sub>, and the photocatalytic activity of CO<sub>2</sub> reduction to CH<sub>3</sub>OH was significantly enhanced under visible light irradiation. NiO extracts the photogenerated electrons from InTaO<sub>4</sub> to reduce the CO<sub>2</sub>. Tsai et al. [91] reported loading Ni@NiO co-catalysts with the core-shell structure to InTaO<sub>4</sub> for photocatalytic CO<sub>2</sub> reduction to CH<sub>3</sub>OH. Ni@NiO NPs induce the transfer of photogenerated electrons from InTaO<sub>4</sub> to Ni@NiO and improve the photocatalyst activity.

#### 4.3. Graphene Co-Catalysts

Carbon materials were the most widespread and infinitely promising materials on earth, ranging from amorphous carbon black to crystalline structured natural layered graphite and from fullerenes with zero-dimensional nanostructures to graphene with two-dimensional structures. Carbon nanomaterials have been attracting significant attention in recent decades. The discovery of graphene self-assembled hydrogels with three-dimensional mesh structures has dramatically enriched the family of carbon materials and provided a new growth point in the field of new materials. It has also shown great scientific significance and experimental results due to its unique nanostructure and properties. Thus, it provides a new goal and direction for researching carbon-based materials.

Photocatalysis could convert light energy into chemical energy for air purification and degradation of organic pollutants in wastewater. It was shown that graphene was compounded with semiconductor photocatalysts, and the regular two-dimensional planar structure of graphene was used as the carrier of photocatalysts. On the one hand, it could improve the dispersion of the catalyst. On the other hand, it could accelerate the photogenerated charge migration rate and improve the composite's photocatalytic activity.

Currently, there are three main methods to improve the photocatalytic efficiency of graphene: mixed method, encapsulation method, and a method with graphene itself involved in a photocatalytic reaction, which are described below.

#### 4.3.1. Composite Method

Graphene oxide (RGO) is known for its two-dimensional and planar conjugate structure, which gives it excellent electron conductivity. The compounding of graphene with photocatalytic materials was a common method to improve photocatalytic efficiency [92]. Sim et al. deposited Pt nanoparticles (Pt NPs) and RGO on the surface of TiO<sub>2</sub> nanotube arrays (TNTs), considering the electron capture function of graphene [93]. Initially, the electron–hole pair recombination time ( $10^{-9}$  s) was faster than the adsorption kinetics of CO<sub>2</sub> molecules on TiO<sub>2</sub>. After depositing RGO sheets on the surface of Pt-TNT, RGO acts as an electron reservoir by trapping photogenerated electrons to inhibit electron–hole pair recombination, while the LSPR effect of Pt-NP enables the composite to have visible light-capturing properties. The quenching of PL spectra, transient photocurrent response, and EIS test reflect the excellent electron–hole pair separation in the photocatalyst due to the coexistence of RGO and Pt-NP. The total methane yield obtained by RGO/Pt-TNTs reached  $10.96 \mu\text{mol}\cdot\text{m}^{-2}$ .

In addition, graphene is also usually combined with non-noble metals as a co-catalyst. Shown et al. synthesized a series of copper nanoparticles (NPs) modified graphene oxide photocatalysts by a simple microwave process, which significantly improved the yield of photocatalytic solar fuel [94]. The results show that with the increase of Cu load, the electrons spontaneously transfer from GO to Cu NP, resulting in the Fermi energy level moving to a more negative potential. Since the Fermi energy level of Cu NP is lower than that of the CB of GO, the photoexcited electrons can be easily transferred from GO to Cu NP while the photogenerated holes remain in the VB of GO. The electrons accumulated on Cu NPs participate in the CO<sub>2</sub> reduction reaction, while the holes in GO participate in the oxidation reaction. This charge transfer mechanism accelerates the charge separation at the interface between GO and Cu NPs, thus inhibiting the recombination of carriers and enhancing the reduction performance of photocatalysts. When the load of Cu NPs is 10 wt%, the solar fuel production rate under visible light reaches the highest value of  $6.84 \mu\text{mol g-cat}^{-1} \text{h}^{-1}$ , more than 60 times the original GO and 240 times the P-25.

Similarly, when compounded with other materials, such as TaON, the band gap width was reduced to a certain extent. There may be strong interactions between graphene and other semiconductor materials, which will increase the Fermi level of graphene. The energy barrier for supplying electrons from graphene to the adsorbed CO<sub>2</sub> is reduced, thus weakening the C=O bond of CO<sub>2</sub> and causing the bond to break.

#### 4.3.2. Wrapping Method

The wrapping method solves the problem of additives causing an increase in the concentration of defects in the catalyst crystal itself. This is because the catalytic efficiency of the photocatalyst is influenced by the thickness of the cladding layer, which is mainly used to adjust the catalyst's light absorption effect by adjusting the cladding layer's thickness [95]. The wrapping method does not change the band gap width of the photocatalyst, so the problem of increasing defect concentration during the crystallization of the catalyst can be adjusted by the wrapping method. The thickness of the catalyst cladding layer should be controlled reasonably during the preparation of the catalyst. The probability of electron–hole complexation can be reduced, which improves photocatalytic activity [96].

#### 4.3.3. Participation of Graphene Itself in Photocatalytic Reactions

The previous two methods introduced different active components, both of which have some degree of influence on the defect concentration in the crystal. Graphene itself has the advantage of fast carrier transport and low charge recombination rate of the photocatalyst. In addition, GO has a wide band gap energy and great potential as a photocatalyst to reduce carbon dioxide to valuable products such as methane, methanol, and formic acid. Therefore, researchers began considering using pure graphene as a catalyst to participate in the photocatalytic reaction.

Kuang et al. prepared two radiation catalysts (GOSS and GOUV) by simulating sunlight (SS) and ultraviolet light (UV) irradiating graphene (GO) [97]. Research shows that radiation has two effects on graphene. On the one hand, radiation eliminated CO released by photolysis in the photocatalytic reaction. On the other hand, radiation activates graphene oxide. Specifically, the radiation caused the generation of defects in GO and restored the large  $\pi$ -conjugation network, making the GO obtain photolytic saturation and sufficient activity to reduce  $\text{CO}_2$ . Irradiated graphene oxide significantly improves the efficiency of photocatalytic reduction of  $\text{CO}_2$ , especially the CO yield of GOSS irradiated under simulated sunlight, which is nearly three times that of original graphene oxide. Although graphene has made some achievements in reducing  $\text{CO}_2$  as a photocatalyst, there are few relevant studies and many problems to be solved.

The following table summarizes a comparison of the photocatalyst performance of different co-catalysts (Table 2).

**Table 2.** Co-catalysts for photocatalytic  $\text{CO}_2$  reduction of metals and non-metals.

Co-Catalysts	Representational Preparation Method	Nitrogen Source	Major $\text{CO}_2$ Reduction Products	Reaction Medium	References
Pt-based	Situ photodeposition, impregnation–calcination and microwave-assisted solvent-heat methods	$\text{N}_2$	$\text{CH}_4$ $\text{CO}$	$\text{H}_2\text{O}$	[15,19]
Ag-based	Sol-gel	$\text{N}_2$	$\text{CH}_4$	$\text{H}_2\text{O}$	[79]
Alloy	Photodeposition	$\text{N}_2$	$\text{C}_2\text{H}_4$ $\text{C}_2\text{H}_6$	$\text{H}_2\text{O}$	[44,45]
Pd-based	Photodeposition	$\text{N}_2$	$\text{CH}_4$ $\text{C}_2\text{H}_6$	$\text{H}_2\text{O}$	[33]
Cu-based	Thermal hydrolysis	$\text{N}_2$	$\text{CH}_3\text{OH}$ $\text{CO}$	$\text{H}_2\text{O}$	[83,84]
Ni-based	Incipient wetness impregnation	$\text{N}_2$	$\text{CH}_3\text{OH}$	$\text{H}_2\text{O}$	[90,91]
Graphene	Hydrothermal method	$\text{N}_2$	$\text{CH}_4$	$\text{H}_2\text{O}$	[92,93]

#### 4.4. Single-Atom Co-Catalysts

The high cost and environmental pollution of photocatalysts limit their application in industrial processes. Nevertheless, using single-atom co-catalysts is an interesting approach to solving this series of problems. Jiang et al. [98] loaded atomically dispersed Cu onto ultrathin  $\text{TiO}_2$  nanosheets (Figure 5), which could reduce  $\text{CO}_2$  to CO. The catalyst also has excellent stability, can be recycled, and is non-polluting to the environment (Figure 6). This technology provides support for green conversion technologies for solar energy.

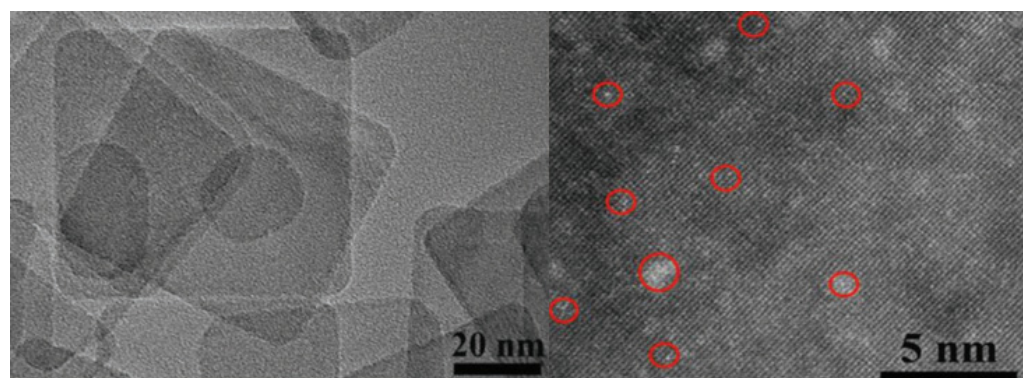


**Figure 5.** TEM image of Cu- $\text{TiO}_2$  photocatalyst [96]. The red circles in the diagram indicate the atomically dispersed Cu.

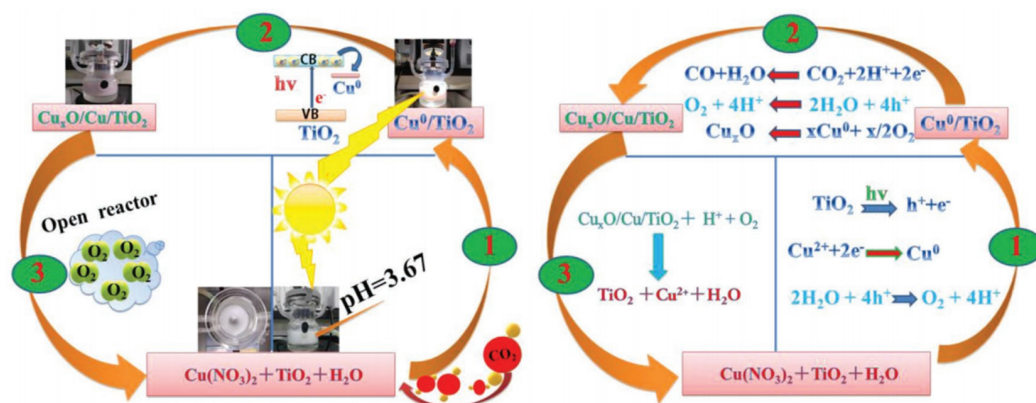


**Figure 6.** Mechanism of CO<sub>2</sub> reduction by Cu dispersed on TiO<sub>2</sub> nanoflakes [96].

Table 3 shows the abbreviations of terms in the manuscript.

**Table 3.** Abbreviations of professional terms.

Names	Abbreviations
Density functional theory	DFT
Ultraviolet photoelectron spectroscopy	UPS
Nanotube arrays	NTAs
Nanotetrahydrogen	NT
Energy dispersive X-ray	EDX
Periodically modulated double-walled titanium dioxide nanotubes	PMTiNT
Reduced graphene oxide	RGO

A number of specialized words appear in the manuscript, and the following table shows the abbreviations of the professional terms (Table 3).

## 5. Challenges and Perspectives

In conclusion, selecting a high activity, selectivity, and stability is necessary to improve CO<sub>2</sub> reduction activity. The co-catalysts have several properties: (1) promoting the separation of photoexcited electron–hole pairs, (2) inhibiting side reactions, and (3) improving the selectivity of target products.

Currently, about half of the literature reports the use of noble metal-based co-catalysts (e.g., Pt-, Au-, and Ag-) and alloys (i.e., Au/Cu and Pt/Cu) for facilitating photocatalytic CO<sub>2</sub> reduction reactions. Recently, researchers have also developed many noble metal-free co-catalysts to aid in the photocatalytic reduction of CO<sub>2</sub>, such as Cu-, Ni-, and graphene. Among them, Cu-based co-catalysts are the most commonly used catalysts for the photocatalytic reduction of CO<sub>2</sub>. Loading a co-catalyst on the surface of the semiconductor is a technology to improve the synergistic effect of CO<sub>2</sub> reduction. However, many results on high activity, stability, and selectivity of catalysts for CO<sub>2</sub> reduction have been reported in the literature. However, it is still in the initial stage of exploration, and there is still much room for development in the future. Several issues are cited below. The activity, stability, and selectivity of co-catalyst-loaded semiconductor catalysts have been studied more in the literature. However, the physicochemical properties, catalytic activity, and coupling of multi-electron and multi-metal reaction mechanisms of co-catalysts have been less studied. In addition, theoretical calculations (e.g., density functional theory) are needed to study the process of CO<sub>2</sub> reduction to provide theoretical knowledge for photocatalytic CO<sub>2</sub> reduction. Unlike other literature, this paper is optimistic about the application prospect of graphene photocatalytic CO<sub>2</sub> reduction for the following two reasons: (1) Graphene has excellent electrical conductivity and large specific surface, so it could improve the available semiconductor materials with low visible light utilization and high excitation electron–hole

complex probability. (2) Graphene is a good co-catalyst for the environment and causes no pollution to the environment before and after the reaction. In future research, we should focus on the direction of graphene photocatalytic CO<sub>2</sub> reduction.

## 6. Conclusions

1. The activity of CO<sub>2</sub> reduction could be improved by controlling the preparation of the catalyst. Currently, monometallic and bimetallic co-catalysts are the most studied in the literature, but there are few studies on three or more polymetallic co-catalysts. In future research, we should focus on developing multi-metal and multi-functional co-catalysts. Finally, it must be noted that co-catalysts that require environmental friendliness, energy efficiency, and other advantages are essential to achieve the scale of industrial application of photocatalysts.
2. We aimed to explore high selectivity, high activity, and low-cost co-catalysts. According to previous studies, catalysts like Cu/Pt and Cu/Au are more effective for CO<sub>2</sub> reduction. Given this, it could be tried to find new and more efficient photocatalysts, such as three metals or metal oxides of more than three metals, metal nitride, metal phosphide, bentonite, spinel, and chalcocite. Multi-component active ingredients with synergistic effects could enhance photocatalytic CO<sub>2</sub> activity. In addition, the stability of semiconductor photocatalysts is also a significant challenge. Finding effective techniques to stop the chemical or photocorrosion of co-catalysts will be a crucial direction for future research.

**Author Contributions:** Methodology, Q.S.; Project Administration, X.Y.; Writing—Original Draft Preparation, C.Z.; Writing—Review and Editing, C.Z. and Q.S.; Validation, C.Z., Q.S., and X.Y. All authors have read and agreed to the published version of the manuscript.

**Funding:** Support for carrying out this work was provided by Natural Science of Shandong Province, China (ZR2021QB214) and the Doctoral Research Foundation of Weifang University, China (2022BS13 and 2021BS48).

**Data Availability Statement:** Not applicable.

**Conflicts of Interest:** The authors declare no conflict of interest.

## References

1. Habisreutinger, S.N.; Schmidt-Mende, L.; Stolarczyk, J.K. Photocatalytic Reduction of CO<sub>2</sub> on TiO<sub>2</sub> and Other Semiconductors. *Angew. Chem. Int. Ed.* **2013**, *52*, 7372–7408. [[CrossRef](#)] [[PubMed](#)]
2. Karamian, E.; Sharifnia, S. On the general mechanism of photocatalytic reduction of CO<sub>2</sub>. *J. CO<sub>2</sub> Util.* **2016**, *16*, 194–203. [[CrossRef](#)]
3. Mao, J.; Li, K.; Peng, T. Recent advances in the photocatalytic CO<sub>2</sub> reduction over semiconductors. *Catal. Sci. Technol.* **2013**, *3*, 2481–2498. [[CrossRef](#)]
4. Cook, J.; Oreskes, N.; Doran, P.T.; Anderegg, W.R.L.; Verheggen, B.; Maibach, E.W.; Carlton, J.S.; Lewandowsky, S.; Skuce, A.G.; Green, S.A.; et al. Consensus on consensus: A synthesis of consensus estimates on human-caused global warming. *Environ. Res. Lett.* **2016**, *11*, 048002. [[CrossRef](#)]
5. Feng, Y.; Wang, C.; Cui, P. Ultrahigh Photocatalytic CO<sub>2</sub> Reduction Efficiency and Selectivity Manipulation by Single-Tungsten-Atom Oxide at the Atomic Step of TiO<sub>2</sub>. *Adv. Mater.* **2022**, *34*, 2109074. [[CrossRef](#)] [[PubMed](#)]
6. Choi, K.M.; Kim, D.; Rungtaweeworanit, B.; Trickett, C.A.; Barmanbek, J.T.; Alshammari, A.S.; Yang, P.; Yaghi, O.M. Plasmon-enhanced photocatalytic CO<sub>2</sub> conversion within metal-organic frameworks under visible light. *J. Am. Chem. Soc.* **2017**, *139*, 356–362. [[CrossRef](#)] [[PubMed](#)]
7. Gondal, M.A.; Dastageer, M.A.; Oloore, L.E.; Baig, U. Laser induced selective photo-catalytic reduction of CO<sub>2</sub> into methanol using In<sub>2</sub>O<sub>3</sub>-WO<sub>3</sub> nano-composite. *J. Photochem. Photobiol. A* **2017**, *343*, 40–50. [[CrossRef](#)]
8. Liu, J.; Liu, M.; Yang, X.L.; Chen, H.; Liu, S.Z.F.; Yan, J.Q. Photo-Redeposition Synthesis of Bimetal Pt–Cu Co-catalysts for TiO<sub>2</sub> Photocatalytic Solar-Fuel Production. *ACS Sustain. Chem. Eng.* **2019**, *6*, 1900289. [[CrossRef](#)]
9. Yu, J.; Low, J.; Xiao, W.; Zhou, P.; Jaroniec, M. Enhanced photocatalytic CO<sub>2</sub> reduction activity of anatase TiO<sub>2</sub> by coexposed {001} and {101} facets. *J. Am. Chem. Soc.* **2014**, *136*, 8839–8842. [[CrossRef](#)]
10. Pu, Y.; Luo, Y.; Wei, X.; Sun, J.; Li, L.; Zou, W.; Dong, L. Synergistic effects of Cu<sub>2</sub>O-decorated CeO<sub>2</sub> on photocatalytic CO<sub>2</sub> reduction: Surface Lewis acid/base and oxygen defect. *Appl. Catal. B* **2019**, *254*, 580–586. [[CrossRef](#)]
11. Nguyen, N.H.; Wu, H.Y.; Bai, H. Photocatalytic reduction of NO<sub>2</sub> and CO<sub>2</sub> using molybdenum-doped titania nanotubes. *Chem. Eng. J.* **2015**, *269*, 60–66. [[CrossRef](#)]

12. Zhang, Z.; Wang, Z.; Cao, S.-W.; Xue, C. Au/Pt Nanoparticle-Decorated TiO<sub>2</sub> Nanofibers with Plasmon-Enhanced Photocatalytic Activities for Solar-to-Fuel Conversion. *J. Phys. Chem. C* **2013**, *117*, 25939–25947. [[CrossRef](#)]
13. Uner, D.; Oymak, M.M. On the mechanism of photocatalytic CO<sub>2</sub> reduction with water in the gas phase. *Catal. Today* **2012**, *181*, 82–88. [[CrossRef](#)]
14. Xiong, Z.; Wang, H.; Xu, N.; Li, H.; Fang, B.; Zhao, Y.; Zhang, J.; Zheng, C. Photocatalytic reduction of CO<sub>2</sub> on Pt<sup>2+</sup>-Pt<sup>0</sup>/TiO<sub>2</sub> nanoparticles under UV/Vis light irradiation: A combination of Pt<sup>2+</sup> doping and Pt nanoparticles deposition. *Int. J. Hydrogen Energy* **2015**, *40*, 10049–10062. [[CrossRef](#)]
15. Xie, S.; Wang, Y.; Zhang, Q.; Deng, W.; Wang, Y. MgO- and Pt-Promoted TiO<sub>2</sub> as an Efficient Photocatalyst for the Preferential Reduction of Carbon Dioxide in the Presence of Water. *ACS Catal.* **2014**, *4*, 3644–3653. [[CrossRef](#)]
16. Dukovic, G.; Merkle, M.G.; Nelson, J.H.; Hughes, S.M.; Alivisatos, A.P. Photodeposition of Pt on Colloidal CdS and CdSe/CdS Semiconductor Nanostructures. *Adv. Mater.* **2008**, *20*, 4306–4311. [[CrossRef](#)]
17. Maimaitizi, H.; Abulizi, A.; Kadeer, K.; Talifu, D.; Tursun, Y. In situ synthesis of Pt and N co-doped hollow hierarchical BiOCl microsphere as an efficient photocatalyst for organic pollutant degradation and photocatalytic CO<sub>2</sub> reduction. *Appl. Surf. Sci.* **2020**, *502*, 144083. [[CrossRef](#)]
18. Fang, B.; Bonakdarpour, A.; Reilly, K.; Xing, Y.; Taghipour, F.; Wilkinson, D.P. Large-scale synthesis of TiO<sub>2</sub> microspheres with hierarchical nanostructure for highly efficient photodriven reduction of CO<sub>2</sub> to CH<sub>4</sub>. *ACS Appl. Mater. Interfaces* **2014**, *6*, 15488–15498. [[CrossRef](#)] [[PubMed](#)]
19. Zhao, Y.; Wei, Y.; Wu, X.; Zheng, H.; Zhao, Z.; Liu, J.; Li, J. Graphene-wrapped Pt/TiO<sub>2</sub> Photocatalysts with Enhanced Photogenerated Charges Separation and Reactant Adsorption for High Selective Photoreduction of CO<sub>2</sub> to CH<sub>4</sub>. *Appl. Catal. B* **2018**, *226*, 360–372. [[CrossRef](#)]
20. Feng, X.; Sloppy, J.D.; LaTempa, T.J.; Paulose, M.; Komarneni, S.; Bao, N.; Grimes, C.A. Synthesis and deposition of ultrafine Pt nanoparticles within high aspect ratio TiO<sub>2</sub> nanotube arrays: Application to the photocatalytic reduction of carbon dioxide. *J. Mater. Chem.* **2011**, *21*, 13429–13433. [[CrossRef](#)]
21. Li, K.; Peng, T.; Ying, Z.; Song, S.; Zhang, J. Ag-loading on brookite TiO<sub>2</sub> quasi nanocubes with exposed {210} and {001} facets: Activity and selectivity of CO<sub>2</sub> photoreduction to CO/CH<sub>4</sub>. *Appl. Catal. B* **2016**, *180*, 130–138. [[CrossRef](#)]
22. Takayama, T.; Tanabe, K.; Saito, K.; Iwase, A.; Kudo, A. The KCaSrTa<sub>5</sub>O<sub>15</sub> photocatalyst with tungsten bronze structure for water splitting and CO<sub>2</sub> reduction. *Phys. Chem. Chem. Phys.* **2014**, *16*, 24417–24422. [[CrossRef](#)]
23. Wang, Z.; Teramura, K.; Huang, Z.; Hosokawa, S.; Sakatad, Y.; Tanaka, T. Tuning the selectivity toward CO evolution in the photocatalytic conversion of CO<sub>2</sub> by H<sub>2</sub>O through the modification of Ag-loaded Ga<sub>2</sub>O<sub>3</sub> with a ZnGa<sub>2</sub>O<sub>4</sub> layer. *Catal. Sci. Technol.* **2016**, *6*, 1025–1032. [[CrossRef](#)]
24. Wang, Z.; Teramura, K.; Hosokawa, S.; Tanaka, T. Highly efficient photocatalytic conversion of CO<sub>2</sub> into solid CO using H<sub>2</sub>O as a reductant over Ag-modified ZnGa<sub>2</sub>O<sub>4</sub>. *J. Mater. Chem. A* **2015**, *3*, 11313–11319. [[CrossRef](#)]
25. Yamamoto, M.; Yoshida, T.; Yamamoto, N.; Nomoto, T.; Yamamoto, Y.; Yagi, S.; Yoshida, H. Photocatalytic reduction of CO<sub>2</sub> with water promoted by Ag clusters in Ag/Ga<sub>2</sub>O<sub>3</sub> photocatalysts. *J. Mater. Chem. A* **2015**, *3*, 16810–16816. [[CrossRef](#)]
26. Ohno, T.; Higo, T.; Murakami, N.; Saito, H.; Zhang, Q.; Yang, Y.; Tsubota, T. Photocatalytic reduction of CO<sub>2</sub> over exposed-crystal-face-controlled TiO<sub>2</sub> nanorod having a brookite phase with co-catalyst loading. *Appl. Catal. B* **2014**, *152–153*, 309–316. [[CrossRef](#)]
27. Zhao, C.; Krall, A.; Zhao, H.; Zhang, Q.; Li, Y. Ultrasonic spray pyrolysis synthesis of Ag/TiO<sub>2</sub> nanocomposite photocatalysts for simultaneous H<sub>2</sub> production and CO<sub>2</sub> reduction. *Int. J. Hydrogen Energy* **2012**, *37*, 9967–9976. [[CrossRef](#)]
28. Wang, Z.; Teramura, K.; Hosokawa, S.; Tanaka, T. Photocatalytic conversion of CO<sub>2</sub> in water over Ag-modified La<sub>2</sub>Ti<sub>2</sub>O<sub>7</sub>. *Appl. Catal. B* **2015**, *163*, 241–247. [[CrossRef](#)]
29. Sui, D.; Yin, X.; Dong, H.; Qin, S.; Chen, J.; Jiang, W. Photocatalytically Reducing CO<sub>2</sub> to Methyl Formate in Methanol over Ag Loaded SrTiO<sub>3</sub> Nanocrystal Catalysts. *Catal. Lett.* **2012**, *142*, 1202–1210. [[CrossRef](#)]
30. Zhang, Y.; Wang, X.; Dong, P.; Huang, Z.; Nie, X.; Zhang, X. TiO<sub>2</sub> Surfaces Self-Doped with Ag Nanoparticles Exhibit Efficient CO<sub>2</sub> Photoreduction under Visible Light. *RSC Adv.* **2018**, *8*, 15991–15998. [[CrossRef](#)]
31. Liu, L.; Pitts, D.T.; Zhao, H.; Zhao, C.; Li, Y. Silver-incorporated bicrystalline (anatase/brookite) TiO<sub>2</sub> microspheres for CO<sub>2</sub> photoreduction with water in the presence of methanol. *Appl. Catal. A* **2013**, *467*, 474–482. [[CrossRef](#)]
32. Yui, T.; Kan, A.; Saitoh, C.; Koike, K.; Ibusuki, T.; Ishitani, O. Photochemical Reduction of CO<sub>2</sub> Using TiO<sub>2</sub>: Effects of Organic Adsorbates on TiO<sub>2</sub> and Deposition of Pd onto TiO<sub>2</sub>. *ACS Appl. Mater. Interfaces* **2011**, *3*, 2594–2600. [[CrossRef](#)]
33. Kim, W.; Seok, T.; Choi, W. Nafion layer-enhanced photosynthetic conversion of CO<sub>2</sub> into hydrocarbons on TiO<sub>2</sub> nanoparticles. *Energy Environ. Sci.* **2012**, *5*, 6066–6070. [[CrossRef](#)]
34. Koci, K.; Matejova, L.; Reli, M.; Capek, L.; Matejka, V.; Lacny, Z.; Kustrowski, P.; Obalbv, L. Sol-Gel Derived Pd Supported TiO<sub>2</sub>ZrO, and TiO, Photocatalysts; Their Examination in PhotocatalyticReduction of Carbon Dioxide. *Catal. Today.* **2014**, *230*, 20–26. [[CrossRef](#)]
35. Hong, J.; Zhang, W.; Wang, Y.; Zhou, T.; Xu, R. Photocatalytic Reduction of Carbon Dioxide over Self-Assembled Carbon Nitride and Layered Double Hydroxide: The Role of Carbon Dioxide Enrichment. *ChemCatChem* **2014**, *6*, 2315–2321. [[CrossRef](#)]
36. Kuai, L.; Chen, Z.; Liu, S.; Kan, E.; Yu, N.; Ren, Y.; Fang, C.; Li, X.; Li, Y.; Geng, B. Titania Supported Synergistic Palladium Single Atoms and Nanoparticles for Room Temperature Ketone and Aldehydes Hydrogenation. *Nat. Commun.* **2020**, *11*, 48. [[CrossRef](#)]

37. Sasirekha, N.; Basha, S.J.S.; Shanthi, K. Photocatalytic performance of Ru doped anatase mounted on silica for reduction of carbon dioxide. *Appl. Catal. B* **2006**, *62*, 169–180. [[CrossRef](#)]
38. Zhang, R.; Wang, H.; Tang, S.; Liu, C.; Dong, F.; Yue, H.; Liang, B. Photocatalytic Oxidative Dehydrogenation of Ethane Using CO<sub>2</sub> as a Soft Oxidant over Pd/TiO<sub>2</sub> Catalysts to C<sub>2</sub>H<sub>4</sub> and Syngas. *ACS Catal.* **2018**, *8*, 9280–9286. [[CrossRef](#)]
39. Yan, S.C.; Ouyang, S.X.; Gao, J.; Yang, M.; Feng, J.Y.; Fan, X.X.; Wan, L.J.; Li, Z.S.; Ye, J.H.; Zhou, Y.; et al. A Room-Temperature Reactive-Template Route to Mesoporous ZnGa<sub>2</sub>O<sub>4</sub> with Improved Photocatalytic Activity in Reduction of CO<sub>2</sub>. *Angew. Chem. Int. Ed.* **2010**, *49*, 6544–6548. [[CrossRef](#)]
40. Yoshino, S.; Sato, K.; Yamaguchi, Y.; Iwase, A.; Kudo, A. Z-schematic CO<sub>2</sub> reduction to CO through interparticle electron transfer between SrTiO<sub>3</sub>: Rh of a reducing photocatalyst and BiVO<sub>4</sub> of a water oxidation photocatalyst under visible light. *ACS Appl. Energy Mater.* **2020**, *3*, 10001–10007. [[CrossRef](#)]
41. Baran, T.; Wojtyła, S.; Dibenedetto, A.; Aresta, M.; Macyk, W. Zinc sulfide functionalized with ruthenium nanoparticles for photocatalytic reduction of CO<sub>2</sub>. *Appl. Catal. B* **2015**, *178*, 170–176. [[CrossRef](#)]
42. Cao, L.; Sahu, S.; Anilkumar, P.; Bunker, C.E.; Xu, J.; Fernando, K.A.S.; Wang, P.; Guliants, E.A., II; Tackett, K.N.; Sun, Y.-P. Carbon Nanoparticles as Visible-Light Photocatalysts for Efficient CO<sub>2</sub> Conversion and Beyond. *J. Am. Chem. Soc.* **2011**, *133*, 4754–4757. [[CrossRef](#)]
43. Rossetti, I.; Villa, A.; Compagnoni, M.; Prati, L.; Ramis, G.; Pirola, C.; Bianchi, C.L.; Wang, W.; Wang, D. CO<sub>2</sub> photoconversion to fuels under high pressure: Effect of TiO<sub>2</sub> phase and of unconventional reaction conditions. *Catal. Sci. Technol.* **2015**, *5*, 4481–4487. [[CrossRef](#)]
44. Wang, J.; Li, G.; Li, Z.; Tang, C.; Feng, Z.; An, H.; Liu, H.; Liu, T.; Li, C. A Highly Selective and Stable ZnO-ZrO<sub>2</sub> Solid Solution Catalyst for CO<sub>2</sub> Hydrogenation to Methanol. *Sci. Adv.* **2017**, *3*, e1701290. [[CrossRef](#)]
45. Zhang, X.; Han, F.; Shi, B.; Farsinezhad, S.; Dechaine, G.P.; Shankar, K. Photocatalytic Conversion of Diluted CO<sub>2</sub> into Light Hydrocarbons Using Periodically Modulated Multiwalled Nanotube Arrays. *Angew. Chem. Int. Ed.* **2012**, *51*, 12732–12735. [[CrossRef](#)]
46. Baldoví, H.G.; Neatu, S.; Khan, A.; Asiri, A.M.; Kosa, S.A.; Garcia, H. Understanding the Origin of the Photocatalytic CO<sub>2</sub> Reduction by Au- and Cu-Loaded TiO<sub>2</sub>: A Microsecond Transient Absorption Spectroscopy Study. *J. Phys. Chem. C* **2015**, *119*, 6819–6827. [[CrossRef](#)]
47. Qin, L.; Si, G.; Li, X.; Kang, S.-Z. Synergetic effect of Cu–Pt bimetallic cocatalyst on SrTiO<sub>3</sub> for efficient photocatalytic hydrogen production from water. *RSC Adv.* **2015**, *5*, 102593–102598. [[CrossRef](#)]
48. Kang, Q.; Wang, T.; Li, P.; Liu, L.; Chang, K.; Li, M.; Ye, J. Photocatalytic Reduction of Carbon Dioxide by Hydrous Hydrazine over Au-Cu Alloy Nanoparticles Supported on SrTiO<sub>3</sub>/TiO<sub>2</sub> Coaxial Nanotube Arrays. *Angew. Chem. Int. Ed.* **2015**, *54*, 841–845. [[CrossRef](#)]
49. Fang, B.; Xing, Y.; Bonakdarpour, A.; Zhang, S.; Wilkinson, D.P. Hierarchical CuO-TiO<sub>2</sub> Hollow Microspheres for Highly Efficient Photodriven Reduction of CO<sub>2</sub> to CH<sub>4</sub>. *ACS Sustain. Chem. Eng.* **2015**, *3*, 2381–2388. [[CrossRef](#)]
50. Ovcharov, M.L.; Mishura, A.M.; Shcherban, N.D.; Filonenko, S.M.; Granchak, V.M. Photocatalytic Reduction of CO<sub>2</sub> using Nanostructured Cu<sub>2</sub>O with Foam-Like Structure. *Sol. Energy* **2016**, *139*, 452–457. [[CrossRef](#)]
51. Zhang, Q.; Gao, T.; Andino, J.M.; Li, Y. Copper and iodine co-modified TiO<sub>2</sub> nanoparticles for improved activity of CO<sub>2</sub> photoreduction with water vapor. *Appl. Catal. B* **2012**, *123–124*, 257. [[CrossRef](#)]
52. Li, Y.; Wang, W.-N.; Zhan, Z.; Woo, M.-H.; Wu, C.-Y.; Biswas, P. Photocatalytic reduction of CO<sub>2</sub> with H<sub>2</sub>O on mesoporous silica supported Cu/TiO<sub>2</sub> catalysts. *Appl. Catal. B* **2010**, *100*, 386. [[CrossRef](#)]
53. Liu, L.; Gao, F.; Zhao, H.; Li, Y. Tailoring Cu valence and oxygen vacancy in Cu/TiO<sub>2</sub> catalysts for enhanced CO<sub>2</sub> photoreduction efficiency. *Appl. Catal. B* **2013**, *134–135*, 349–358. [[CrossRef](#)]
54. Liu, D.; Fernández, Y.; Ola, O.; Mackintosh, S.; Maroto-Valer, M.; Parlett, C.M.A.; Lee, A.F.; Wu, J.C.S. On the impact of Cu dispersion on CO<sub>2</sub> photoreduction over Cu/TiO<sub>2</sub>. *Catal. Commun.* **2012**, *25*, 78. [[CrossRef](#)]
55. Yang, H.-C.; Lin, H.-Y.; Chien, Y.-S.; Wu, J.C.-S.; Wu, H.-H. Mesoporous TiO<sub>2</sub>/SBA-15, and Cu/TiO<sub>2</sub>/SBA-15 Composite Photocatalysts for Photoreduction of CO<sub>2</sub> to Methanol. *Catal. Lett.* **2009**, *131*, 381. [[CrossRef](#)]
56. Wang, W.-N.; Park, J.; Biswas, P. Rapid synthesis of nanostructured Cu-TiO<sub>2</sub>-SiO<sub>2</sub> composites for CO<sub>2</sub> photoreduction by evaporation driven self-assembly. *Catal. Sci. Technol.* **2011**, *1*, 593. [[CrossRef](#)]
57. Liu, E.; Qi, L.; Bian, J.; Chen, Y.; Hu, X.; Fan, J.; Liu, H.; Zhu, C.; Wang, Q. A facile strategy to fabricate plasmonic Cu modified TiO<sub>2</sub> nano-flower films for photocatalytic reduction of CO<sub>2</sub> to methanol. *Mater. Res. Bull.* **2015**, *68*, 203. [[CrossRef](#)]
58. Huang, L.; Duan, Z.; Song, Y.; Li, Q.; Chen, L. BiVO<sub>4</sub> microplates with oxygen vacancies decorated with metallic Cu and Bi nanoparticles for CO<sub>2</sub> photoreduction. *ACS Appl. Nano Mater.* **2021**, *4*, 3576–3585. [[CrossRef](#)]
59. Bharad, P.A.; Nikam, A.V.; Thomas, F.; Gopinath, C.S. CuO<sub>x</sub>-TiO<sub>2</sub> composites: Electronically integrated nanocomposites for solar hydrogen generation. *Chemistryselect* **2018**, *3*, 12022–12030. [[CrossRef](#)]
60. Srinivas, B.; Shubhamangala, B.; Lalitha, K.; Reddy, P.A.K.; Kumari, V.D.; Subrahmanyam, M. Photocatalytic reduction of CO<sub>2</sub> over Cu-TiO<sub>2</sub>/molecular sieve 5A composite. *Photochem. Photobiol.* **2011**, *87*, 995. [[CrossRef](#)]
61. Kumar, A.; Sharma, G.; Naushad, M.; Ahamad, T.; Veses, R.C.; Stadler, F.J. Highly visible active Ag<sub>2</sub>CrO<sub>4</sub>/Ag/BiFeO<sub>3</sub>@RGO nano-junction for photoreduction of CO<sub>2</sub> and photocatalytic removal of ciprofloxacin and bromate ions: The triggering effect of Ag and RGO. *Chem. Eng. J.* **2019**, *370*, 148–165. [[CrossRef](#)]

62. Jeyalakshmi, V.; Mahalakshmy, R.; Krishnamurthy, K.R.; Viswanathan, B. Photocatalytic Reduction of Carbon Dioxide by Water: A Step towards Sustainable Fuels and Chemicals. *Catal. Today* **2016**, *266*, 160. [[CrossRef](#)]
63. Wang, J.; Li, B.; Chen, J.; Li, N.; Zheng, J.; Zhao, J.; Zhu, Z. Enhanced photocatalytic H<sub>2</sub> production activity of Cd<sub>x</sub>Zn<sub>1-x</sub>S nanocrystals by surface loading MS (M = Ni, Co, Cu) species. *Appl. Surf. Sci.* **2012**, *259*, 118–123. [[CrossRef](#)]
64. Ruan, C.; Huang, Z.-Q.; Lin, J.; Li, L.; Liu, X.; Tian, M.; Huang, C.; Chang, C.-R.; Li, J.; Wang, X. Synergy of the catalytic activation on Ni and the CeO<sub>2</sub>–TiO<sub>2</sub>/Ce<sub>2</sub>Ti<sub>2</sub>O<sub>7</sub> stoichiometric redox cycle for dramatically enhanced solar fuel production. *Energy Environ. Sci.* **2019**, *12*, 767–779. [[CrossRef](#)]
65. Liou, P.Y.; Chen, S.C.; Wu, J.C.S.; Liu, D.; Mackintosh, S.; Maroto-Valer, M.; Linforth, R. Photocatalytic CO<sub>2</sub> reduction using an internally illuminated monolith photoreactor. *Energy Environ. Sci.* **2011**, *4*, 1487. [[CrossRef](#)]
66. Miao, Y.F.; Guo, R.T.; Gu, J.W.; Liu, Y.Z.; Wu, G.L.; Duan, C.P.; Pan, W.G. Z-scheme Bi/Bi<sub>2</sub>O<sub>2</sub>CO<sub>3</sub>/Layered double-hydroxide nanosheet heterojunctions for photocatalytic CO<sub>2</sub> reduction under visible light. *ACS Appl. Nano Mater.* **2021**, *4*, 4902–4911. [[CrossRef](#)]
67. Yu, L.; Zhang, X.; Li, G.; Cao, Y.; Shao, Y.; Li, D. Highly efficient Bi<sub>2</sub>O<sub>2</sub>CO<sub>3</sub>/BiOCl photocatalyst based on heterojunction with enhanced dye-sensitization under visible light. *Appl. Catal. B* **2016**, *187*, 301–309. [[CrossRef](#)]
68. Zhang, H.; Wei, J.; Dong, J.; Liu, G.; Shi, L.; An, P.; Zhao, G.; Kong, J.; Wang, X.; Meng, X.; et al. Efficient Visible-Light-Driven Carbon Dioxide Reduction by a Single-Atom Implanted Metal-Organic Framework. *Angew. Chem. Int. Ed.* **2016**, *55*, 14310. [[CrossRef](#)]
69. Wei, L.; Yu, C.; Zhang, Q.; Liu, H.; Wang, Y. TiO<sub>2</sub>-Based Heterojunction Photocatalysts for Photocatalytic Reduction of CO<sub>2</sub> into Solar Fuels. *J. Mater. Chem. A* **2018**, *6*, 22411–22436. [[CrossRef](#)]
70. Nie, N.; Zhang, L.; Fu, J.; Cheng, B.; Yu, J. Self-assembled hierarchical direct Z-scheme g-C<sub>3</sub>N<sub>4</sub>/ZnO microspheres with enhanced photocatalytic CO<sub>2</sub> reduction performance. *Appl. Surf. Sci.* **2018**, *441*, 12–22. [[CrossRef](#)]
71. Zhou, L.; Kamyab, H.; Surendar, A.; Maselena, A.; Ibatova, A.Z.; Chelliapan, S.; Karachi, N.; Parsaee, Z. Novel Z-scheme composite Ag<sub>2</sub>CrO<sub>4</sub>/NG/polyimide as high performance nano catalyst for photoreduction of CO<sub>2</sub>: Design, fabrication, characterization and mechanism. *J. Photochem. Photobiol. A* **2019**, *368*, 30–40. [[CrossRef](#)]
72. Xu, Q.L.; Xia, Z.H.; Zhang, J.M.; Wei, Z.Y.; Guo, Q.; Jin, H.L.; Tang, H.; Li, S.Z.; Pan, X.C.; Su, Z.; et al. Recent advances in solar-driven CO<sub>2</sub> reduction over g-C<sub>3</sub>N<sub>4</sub>-based photocatalysts. *Carbon Energy* **2022**. [[CrossRef](#)]
73. Li, X.; Zhuang, Z.; Li, W.; Pan, H. Photocatalytic reduction of CO<sub>2</sub> over noble metal-loaded and nitrogen-doped mesoporous TiO<sub>2</sub>. *Appl. Catal. A* **2012**, *429–430*, 31–38. [[CrossRef](#)]
74. Kočí, K.; Matějů, K.; Obalová, L.; Krejčíková, S.; Lacný, Z.; Plachá, D.; Čapek, L.; Hospodková, A.; Šolcová, O. Effect of silver doping on the TiO<sub>2</sub> for photocatalytic reduction of CO<sub>2</sub>. *Appl. Catal. B-Environ.* **2013**, *96*, 239–244. [[CrossRef](#)]
75. Yuan, Y.-P.; Cao, S.-W.; Liao, Y.-S.; Yin, L.-S.; Xue, C. Red phosphor/g-C<sub>3</sub>N<sub>4</sub> heterojunction with enhanced photocatalytic activities for solar fuels production. *Appl. Catal. B* **2013**, *140–141*, 164–168. [[CrossRef](#)]
76. Gao, G.; Jiao, Y.; Waclawik, E.R.; Du, A. Single atom (Pd/Pt) supported on graphitic carbon nitride as efficient photocatalyst for visible-light reduction of carbon dioxide. *J. Am. Chem. Soc.* **2016**, *138*, 6292. [[CrossRef](#)]
77. Li, X.; Li, W.; Zhuang, Z.; Zhong, Y.; Li, Q.; Wang, L. Photocatalytic Reduction of Carbon Dioxide to Methane over SiO<sub>2</sub>-Pillared HNb<sub>3</sub>O<sub>8</sub>. *J. Phys. Chem. C* **2012**, *116*, 16047. [[CrossRef](#)]
78. Yu, X.; Wang, Y.; Kim, A.; Kim, Y.K. Observation of Temperature-Dependent Kinetics for Catalytic CO Oxidation over TiO<sub>2</sub>-Supported Pt Catalysts. *Chem. Phys. Lett.* **2017**, *685*, 282–287. [[CrossRef](#)]
79. Asi, M.A.; Zhu, L.; He, C.; Sharma, V.K.; Shu, D.; Li, S.; Yang, J.; Xiong, Y. Visible-Light-Harvesting Reduction of CO<sub>2</sub> to Chemical Fuels with Plasmonic Ag@AgBr/CNT Nanocomposites. *Catal. Today* **2013**, *216*, 268–275. [[CrossRef](#)]
80. Iizuka, K.; Wato, T.; Miseki, Y.; Saito, K.; Kudo, A. Photocatalytic Reduction of Carbon Dioxide over Ag Cocatalyst-Loaded ALa<sub>4</sub>Ti<sub>4</sub>O<sub>15</sub> (A=Ca, Sr, and Ba) Using Water as a Reducing Reagent. *J. Am. Chem. Soc.* **2011**, *133*, 20863. [[CrossRef](#)]
81. Bai, S.; Wang, X.; Hu, C.; Xie, M.; Jiang, J.; Xiong, Y. Two-dimensional g-C<sub>3</sub>N<sub>4</sub>: An ideal platform for examining facet selectivity of metal co-catalysts in photocatalysis. *Chem. Commun.* **2014**, *50*, 6094. [[CrossRef](#)] [[PubMed](#)]
82. Tseng, I.-H.; Wu, J.C.-S. Photoreduction of CO<sub>2</sub> using sol-gel derived titania and titania-supported copper catalysts. *Appl. Catal. B* **2002**, *37*, 37–48. [[CrossRef](#)]
83. Wu, J.C.S.; Wu, T.H.; Chu, T.; Huang, H.; Tsai, D. Application of Optical-fiber Photoreactor for CO<sub>2</sub> Photocatalytic Reduction. *Top. Catal.* **2008**, *47*, 131–136. [[CrossRef](#)]
84. Tseng, I.-H.; Wu, J.C.-S. Effects of sol-gel procedures on the photocatalysis of Cu/TiO<sub>2</sub> in CO<sub>2</sub> photoreduction. *J. Catal.* **2004**, *221*, 432–440. [[CrossRef](#)]
85. Xie, S.; Ma, W.; Wu, X.; Zhang, H.; Zhang, Q.; Wang, Y.; Wang, Y. Photocatalytic and Electrocatalytic Transformations of C1 Molecules Involving C-C Coupling. *Energy Environ. Sci.* **2021**, *14*, 37–89. [[CrossRef](#)]
86. Ajmal, S.; Yang, Y.; Tahir, M.; Li, K.A.; Bacha, A.-U.-R.; Nabi, I.; Liu, Y.; Wang, T.; Zhang, L. Boosting C<sub>2</sub> Products in Electrochemical CO<sub>2</sub> Reduction over Highly Dense Copper Nanoplates. *Catal. Sci. Technol.* **2020**, *10*, 4562–4570. [[CrossRef](#)]
87. Slamet; Nasution, H.W.; Purnama, E.; Kosela, S.; Gunlazuardi, J. Photocatalytic reduction of CO<sub>2</sub> on copper-doped Titania catalysts prepared by improved-impregnation method. *Catal. Commun.* **2005**, *6*, 313. [[CrossRef](#)]
88. Zhao, H.; Duan, J.; Zhang, Z.; Wang, W. Bi-Ti-In trimetallic sites in the Indium-doped Bi<sub>4</sub>Ti<sub>3</sub>O<sub>12</sub>-CuIn<sub>5</sub>S<sub>8</sub> S-scheme heterojunction for controlling the selectivity of CO<sub>2</sub> photoreduction. *Fuel* **2022**, *325*, 124993. [[CrossRef](#)]

89. Adachi, K.; Ohta, K.; Mizuno, T. Photocatalytic reduction of carbon dioxide to hydrocarbon using copper-loaded titanium dioxide. *Sol. Energy* **1994**, *53*, 187. [[CrossRef](#)]
90. Wang, Z.-Y.; Chou, H.-C.; Wu, J.C.; Tsai, D.P.; Mul, G. CO<sub>2</sub> photoreduction using NiO/InTaO<sub>4</sub> in optical-fiber reactor for renewable energy. *Mul. Appl. Catal. A* **2010**, *380*, 172. [[CrossRef](#)]
91. Tsai, C.-W.; Chen, H.M.; Liu, R.-S.; Asakura, K.; Chan, T.-S. Ni@NiO Core-Shell Structure-Modified Nitrogen-Doped InTaO<sub>4</sub> for Solar-Driven Highly Efficient CO<sub>2</sub> Reduction to Methanol. *J. Phys. Chem. C* **2011**, *115*, 10180. [[CrossRef](#)]
92. Li, N.; Jiang, R.; Li, Y.; Zhou, J.; Ma, Q.; Shen, S.; Liu, M. Plasma-Assisted Photocatalysis of CH<sub>4</sub> and CO<sub>2</sub> into Ethylene. *ACS Sustain. Chem. Eng.* **2019**, *7*, 11455–11463. [[CrossRef](#)]
93. Sim, L.C.; Leong, K.H.; Saravanan, P.; Ibrahim, S. Rapid thermal reduced graphene oxide/Pt-TiO<sub>2</sub> nanotube arrays for enhanced visible-light-driven photocatalytic reduction of CO<sub>2</sub>. *Appl. Surf. Sci.* **2015**, *358*, 122–129. [[CrossRef](#)]
94. Shown, I.; Hsu, H.-C.; Chang, Y.-C.; Lin, C.-H.; Roy, P.K.; Ganguly, A.; Wang, C.-H.; Chang, J.-K.; Wu, C.-I.; Chen, L.-C.; et al. Highly Efficient Visible Light Photocatalytic Reduction of CO<sub>2</sub> to Hydrocarbon Fuels by Cu-Nanoparticle Decorated Graphene Oxide. *Nano Lett.* **2014**, *14*, 6097. [[CrossRef](#)] [[PubMed](#)]
95. Yu, J.; Jin, J.; Cheng, B.; Jaroniec, M. A noble metal-free reduced graphene oxide-CdS nanorod composite for the enhanced visible-light photocatalytic reduction of CO<sub>2</sub> to solar fuel. *J. Mater. Chem. A* **2014**, *2*, 3407. [[CrossRef](#)]
96. Gui, M.M.; Chai, S.-P.; Xu, B.-Q.; Mohamed, A.R. Enhanced visible light responsive MWCNT/TiO<sub>2</sub> core-shell nanocomposites as the potential photocatalyst for reduction of CO<sub>2</sub> into methane. *Sol. Energy Mater. Sol. Cells* **2014**, *122*, 183. [[CrossRef](#)]
97. Kuang, Y.; Shang, J.; Zhu, T. Photo-Activated Graphene Oxide to Enhance Photocatalytic Reduction of CO<sub>2</sub>. *ACS Appl. Mater. Interfaces* **2020**, *12*, 3580–3591. [[CrossRef](#)] [[PubMed](#)]
98. Jiang, Z.; Sun, W.; Miao, W.; Yuan, Z. Living Atomically Dispersed Cu Ultrathin TiO<sub>2</sub> Nanosheet CO<sub>2</sub> Reduction Photocatalyst. *Adv. Sci.* **2019**, *6*, 1900289. [[CrossRef](#)]

**Disclaimer/Publisher's Note:** The statements, opinions and data contained in all publications are solely those of the individual author(s) and contributor(s) and not of MDPI and/or the editor(s). MDPI and/or the editor(s) disclaim responsibility for any injury to people or property resulting from any ideas, methods, instructions or products referred to in the content.